

Property Assessment of Hybrid Fiber-Reinforced Ultra-High-Performance Concrete

Piotr Smarzewski¹  · Danuta Barnat-Hunek²

Received: 3 June 2016 / Revised: 7 January 2017 / Accepted: 9 January 2017 / Published online: 16 February 2017
© The Author(s) 2017. This article is published with open access at Springerlink.com

Abstract The purpose of this study was to determine the effect of steel/polypropylene hybrid fibers on the mechanical properties and microstructure of ultra-high-performance concrete (UHPC). Tests were carried out on UHPC without and with fibers (steel and/or polypropylene in amounts of 0.25–1%). In this study, granite or granodiorite coarse aggregate with a grain size of about 2/8 mm was employed. The three-point bending tests displayed prolonged post-peak softening behavior. In addition, increasing the content of polypropylene fibers reduced the fracture energy. Moreover, the SEM results illustrated that adding a certain amount of fibers to concrete considerably changes the microstructure. It was observed that the smallest microcracks in the interfacial transition zone between the paste and aggregate occurred in the concrete containing steel fibers.

Keywords Ultra-high-performance concrete · Hybrid steel/polypropylene fiber · Fracture energy · Microstructure

1 Introduction

Ultra-high-performance concrete (UHPC) is a cement-based material, which has received a great deal of attention around the world, since it was introduced in the

early 1990s [1]. UHPC is characterized by a compressive strength above 120 MPa and high durability [2]. At present, some limitations remain regarding the use of standard concrete, such as its low tensile strength and ductility; however, it is possible that ultra-high-performance concrete reinforced with hybrid fibers can overcome these limitations. The main advantages of the UHPC mixture are: low values of water/binder ratio, the elimination of coarse aggregate, namely, the use of only fine aggregate, a limited amount of fine aggregate, and a packing density in which the grains fill the voids [3]. Besides utilizing a water-reducing agent, an addition of silica fume in UHPC mixtures is recommended to improve the workability [1, 4] as silica fume has a diameter small enough to fill the interstitial voids between the cement and quartz sand particles. What is more, to reduce labor costs and provide architects and designers greater architectural freedom in structural member shapes and forms, it is advisable to either to reduce or completely eliminate the implementation of steel reinforcement bars. Nonetheless, the drawbacks of UHPC are that, on the whole, it is expensive and cannot substitute standard concrete in the majority of applications [5]. It is due to the composition of its mixtures that make the UHPC microstructure different from ordinary concrete. For UHPC at $W/C=0.20$, its capillary pores become discontinuous when only 26% of the cement has been hydrated, instead of 54% for HPC, where $W/C=0.33$ [1, 6]. The pore size of UHPC basically varies between 2 and 3 nm, and its total porosity is 2.23% [1]. Studies on UHPC have been carried out by several researchers; nevertheless, the information on UHPC materials and structural properties is still rather lacking. A great deal of this research has revealed that a combination of steel-polypropylene fibers in concrete could take advantage of the material properties of both the fibers to

✉ Piotr Smarzewski
p.smarzewski@pollub.pl

¹ Department of Structural Engineering, Faculty of Civil Engineering and Architecture, Lublin University of Technology, 40 Nadbystrzycka Str., 20-618 Lublin, Poland

² Department of Construction, Faculty of Civil Engineering and Architecture, Lublin University of Technology, 40 Nadbystrzycka Str., 20-618 Lublin, Poland

Table 1 Cement chemical composition

Cement component	SiO ₂	Al ₂ O ₃	Fe ₂ O ₃	CaO	MgO	SO ₃	Na ₂ O	K ₂ O	Cl	Ignition loss	Ash	Total
Content (wt%)	20.92	3.50	4.38	64.69	1.20	3.07	0.22	0.38	0.082	1.27	0.26	99.97

Table 2 Technical parameters of cement

Cement characteristics	CEM I 52.5 N-HSR/NA
Specific surface area (cm ² /g)	4433
Water demand (%)	30
Commencement of bonding (min)	120
End of bonding (min)	180
Volume stability according to Le Chateliere (mm)	2
Compressive strength after 2 days (MPa)	27.7
Compressive strength after 28 days (MPa)	57.1
Tensile strength after 2 days (MPa)	5.29
Tensile strength after 28 days (MPa)	8.23

Table 3 Properties of coarse aggregates

Aggregate characteristics	Granite	Granodiorite
Density (cm ³ /g)	2.67	2.63
Porosity (%)	0.9	1.13
Absorption, W ₂₄ (%)	0.30	0.32
Ash content (%)	0.02	0.26
Frost resistance, F (%)	0.15	0.36
Resistance to crushing, LA (%)	32	23.4
Resistance to polishing, PSV (%)	53	57.3
Shape factor, SI (%)	14	8.4
Crusher reduction ratio, X _{rm} (%)	15.1	6.0
Los Angeles abrasion (%)	16	23.4

effectively improve the condition of the interface between the cement and aggregate by restricting the incidence and development of concrete cracks [1, 7, 8]. Therefore, to do this, as well as improve the general ductility of the material, the matrix is reinforced by an addition of fibers [9, 10]. Some concrete properties can be enhanced by adding polypropylene or steel fibers. Usually, to improve the mechanical and physical properties, especially the tensile strength, flexural strength, and long-term concrete shrinkage, steel fibers are used. On the other hand, polypropylene fibers are more advantageous thanks to the fact that they do not corrode, and are thermally stable, chemically inert and very stable in the alkaline environment of concrete [11, 12]. Moreover, polypropylene has a hydrophobic surface—it does not absorb water nor it does interfere in the concrete hydration reaction [13]. Nonetheless, owing to drying shrinkage in hardened concrete, cracks generally develop over time which weaken the waterproofing capabilities and expose the concrete microstructure to destructive substances [14–16]. Therefore, a chief aim in concrete science is to enhance the properties of hardened concrete [17]. Factors, such as the fiber–matrix properties, fiber geometry, volume of fiber inclusion, type of fiber, and fiber orientation in the concrete mixture, determine fiber efficiency [14, 18–20]. Hence, applying different fibers of various lengths and qualities is a useful method to resolve the issue of cracks of assorted sizes appearing at various stages of concrete structure exploitation. The reason for the better performance of hybrid fiber-reinforced concrete than one with a single kind of fibers is the favorable interaction between the fibers and the concrete [21, 22]. Controlling cracks of assorted sizes

and in various zones of the cementitious material is the principal motivation for combining diverse types of fibers [23].

The purpose of this study is to assess the properties of hybrid fiber-reinforced UHPC. To this aim, compressive and splitting tensile strength tests on cube specimens, static and dynamic moduli of elasticity tests on cylinders and three-point bending tests on notched samples [24, 25] were carried out. The fracture energy values were compared. The interfacial transition zone between the paste and aggregate of fiber-reinforced UHPC was investigated by scanning electron microscope (SEM) analysis.

2 Experimental Procedure

2.1 Material Specification

Portland cement CEM I 52.5, silica fume, quartz sand, granite, granodiorite, water, superplasticizer, steel fibers, and polypropylene fibers were used in the UHPC mixes. The cement properties were determined according to PN-EN 197-1:2002 and PN-B-19707:2013-10. The composition and technical parameters are presented in Tables 1 and 2, respectively.

The particle size distribution for the granodiorite and granite aggregate as well as quartz sand was determined based on standard PN-EN 933-1:2000. The physical and mechanical properties of the coarse aggregates are shown in Table 3.

The polypropylene fibers (PF) had a diameter of 25 μm, length of 12 mm, and a modulus of elasticity of 3.5 GPa.

Hooked-end steel fibers (SF) 50 mm long (aspect ratio of 50), with a modulus of elasticity of 200 GPa, and tensile strength of 1100 MPa were applied. A superplasticizer based on polycarboxylate ethers was used.

2.2 Mixtures and Sample Production Process

The concrete mixtures were prepared using: Portland cement CEM I 52.5 N-HSR/NA 670.5 kg/m³, granodiorite 2/8 mm or granite 2/8 mm aggregate 990 kg/m³, quartz sand 0/2 mm 500 kg/m³, water 178 l/m³, silica fume 74.5 kg/m³, superplasticizer 20 l/m³, and quantities of steel and polypropylene fibers which varied in percentage. In the first three concrete mixes—granodiorite aggregate was used, and in the remaining four—granite aggregate. In Table 4, the abbreviated concrete types and quantities of steel and polypropylene fibers for various batches are displayed.

At the beginning of mixing, the coarse aggregate and sand were homogenized with a half of the quantity of water. Subsequently, cement, silica fume, the remaining water, and the superplasticizer were added. The fibers were added by hand after having thoroughly mixed the ingredients. Samples were formed directly after all the compounds were mixed. Moulds coated with an anti-adhesive substance were filled and compacted. All the samples were stored at a temperature of about 23 °C until they were removed from the moulds after 24 h, and then, they were placed in a water tank for 7 days to cure. After 7 days, the samples were removed from the tank to cure to 28 days.

2.3 Test Methods

Experimental examinations were carried out on cubes, cylinders, and notched prismatic samples made from UHPC and fiber-reinforced UHPC with varying contents of steel fibers (SF) and/or polypropylene fibers (PF). Compressive strength, splitting tensile strength, static modulus of elasticity, dynamic modulus of elasticity, flexural tensile strength, and three-point bending tests were conducted to ascertain

the impact of the fiber type and its content on the compressive and tensile behavior, deflection, as well as fracture energy.

2.4 Test Equipment and Solutions

2.4.1 Compressive and Splitting Tensile Strength

The compressive strength and splitting tensile strength were determined after 28 days on 100 mm × 100 mm × 100 mm cubes, based on PN-EN 12390-3:2002 and PN-EN 12390-6:2001. A hydraulic machine was employed.

2.4.2 Static and Dynamic Moduli of Elasticity

Testing of the static and dynamic moduli of elasticity was carried out on cylinders 150 mm in diameter and 300 mm in height. The static modulus tests were conducted using a device with an extensometer according to ASTM C469-02:2004. The dynamic modulus was determined using the method based on resonance frequency measurements.

The test of dynamic modulus of elasticity was conducted based on ASTM C666 and ASTM C215. A steel ball 10 mm in diameter was used as the impact source. The ball hits the top surface of the cylindrical specimen, the accelerometer measured the vertical motion, and the data were obtained. The dynamic modulus of elasticity was calculated by means of the formula $E_{DM} = 4L^2n^2\rho$ (GPa), where: L is the specimen length (m), n is the frequency (kHz), and ρ is the apparent density (kg/m³) [26].

2.4.3 Flexural Tensile Strength

The flexural tensile strength test was performed on specimens 100 mm × 100 mm × 500 mm. The investigations were conducted according to EN 12390-5:2009. Testing was performed after 28 days. The samples were loaded with a centrally placed force. Spacing of the supports was 300 mm.

Table 4 Percentage of fibers

Type of concrete	Mass (kg/m ³)		Percentage (%)	
	Polypropylene fibers PF	Steel fibers SF	Polypropylene fibers PF	Steel fibers SF
C1	–	–	–	–
SC	–	78	–	1
SPC1	2.25	58.5	0.25	0.75
SPC2	4.5	39	0.5	0.5
SPC3	6.75	19.5	0.75	0.25
PC	9	–	1	–
C2	–	–	–	–

2.4.4 Fracture Energy

Three-point bending tests were carried out after 28 days using notched specimens with the dimensions 80 mm × 150 mm × 700 mm, based on RILEM TC 89-FMT (Fig. 1), setting a displacement rate of 0.05 mm/min. A notch with a depth of 50 mm and a thickness of 3 mm was

made in the mid-span by a flat iron with a sharpened tip. Two plates were glued at the notch to fix the gauge clip.

The equations for computing stress intensity factor K_{Ic} which describes the stress field near the tip of a crack, and fracture energy G_F for C1 and C2 UHPC without fibers are given in Table 5 [27]. These factors are used to ascertain the stress–strain curves for modelling UHPC and

Fig. 1 Three-point bending tests on notched specimens: **a** set-up, **b** notched samples after test, and **c** cross section of break point of samples without/with fibers

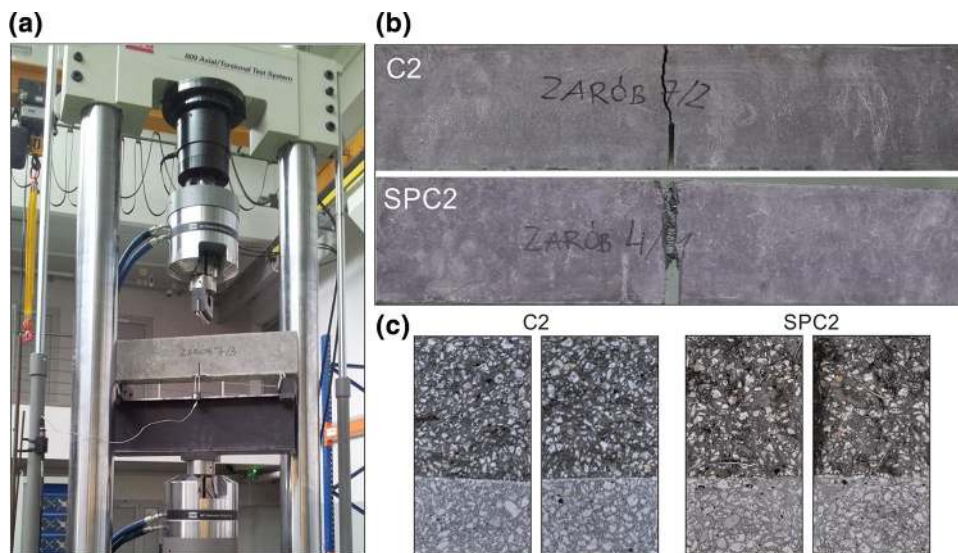


Table 5 Equations for determining tensile strength parameters and fracture energy

Strength parameters	Equation
UHPC	
Stress intensity factor	$K_{Ic} = \frac{F_{max}}{b\sqrt{h}} f(\alpha)$ (MN/m ^{1.5})
Geometry function	$f(\alpha) = 6\sqrt{\alpha} \left\{ \frac{1.99 - \alpha(1 - \alpha)(2.15 - 3.93\alpha + 2.7\alpha^2)}{(1 + 2\alpha)(1 - \alpha)^{3/2}} \right\}$
Fracture energy	$G_F = \frac{K_{Ic}^2(1 - \nu)}{E_{cm}}$ (N/mm)
Fiber-reinforced UHPC	
Strength corresponding to limit of proportionality	$f_{i,ct,L} = \frac{3F_{i,L}l}{2b(h - a_0)^2}$ (MPa)
Equivalent flexural strength	$f_{eq,2} = \frac{3l}{2b(h - a_0)^2} \frac{A_2}{0.5}$ (MPa)
	$f_{eq,3} = \frac{3l}{2b(h - a_0)^2} \frac{A_3}{2.5}$ (MPa)
Residual flexural strength $f_{R,1}$ and $f_{R,4}$ at mid-span deflection of 0.46 mm and 3 mm	$f_{R,1} = \frac{3F_{R,1}l}{2b(h - a_0)^2}$ (MPa)
	$f_{R,4} = \frac{3F_{R,4}l}{2b(h - a_0)^2}$ (MPa)
Tensile stress	$\sigma = \frac{3Fl}{2b(h - a_0)^2}$ (MPa)
Fracture energy	$G_F = \int_{\delta=0}^{\delta=\delta_{lim}} \sigma d\delta$ (N/mm)

F_{max} is the critical force, b is the sample width ($b = 80$ mm), h is the sample height ($h = 150$ mm), α is the relative crack length, $\alpha = a_0/h$, a_0 is the notch depth ($a_0 = 50$ mm), ν is Poisson's ratio, E_{cm} is the average static modulus of elasticity, l is the sample span ($l = 600$ mm), $(h - a_0)$ is the distance between the tip of the notch and the top edge of the sample, F is the load recorded during the three-point bending test

fiber-reinforced UHPC post-cracking behavior. RILEM recommendation TC162-TDF [28] has been backed by several research centers that investigated deflection variability using the crack mouth opening displacement (CMOD) and fiber distribution in particular sample sections [29–31]. Toughness indexes were recommended (equivalent flexural tensile strength— f_{eq} and residual flexural tensile strength— f_R) to define amelioration after cracking for fiber-reinforced UHPC [32, 33]. According to RILEM, $f_{eq,2}$ or $f_{R,1}$ is employed to verify the serviceability limit states, whereas $f_{eq,3}$ or $f_{R,4}$ is applied in the ultimate limit states [28]. Load F_L is equal to the load recorded up to a deflection of 0.05 mm. Factors $f_{eq,2}$ and $f_{eq,3}$ were assessed up to a deflection of $\delta_2 = \delta_L + 0.65$ mm and $\delta_3 = \delta_L + 2.65$ mm, where δ_L is the deflection consistent with F_L . The equations for computing the flexural tensile strength parameters and fracture energy for fiber-reinforced UHPC are shown in Table 5.

2.4.5 Microstructure Investigations

Microstructural investigations were carried out using an FEI Quanta 250 FEG scanning electron microscope (SEM) equipped with a chemical compounds analysis system based on energy dispersive spectrometry (EDS). Six samples from each UHPC batch were prepared as thin-layer plates. Measurements of the micro-cracks in the interfacial transition zone enabled estimation of the average width of the micro-cracks. The average value of micro-crack width was calculated after analyzing 15 SEM images and 30 measurements of representative crack widths for each type of UHPC.

3 Experimental Results

3.1 Compressive Strength

The average values and error bars of cube compressive strength are given in Fig. 2.

Adding SF and PF did not have a considerable impact on the cube compressive strength; however, a greater drop in compressive strength with a higher percentage of PF volume was observed, mainly due to some difficulties in dispersing the polypropylene fibers in the mixes, as well as the low modulus of elasticity for this fiber. The strength of the C2 cubes was 57.3% higher than the PC strength with a 1% PF volume content made with granite aggregate. The cube strength made of SPC3 was about 5.5% lower than that of C2. The highest compressive strength was exhibited by the SC concrete with granodiorite aggregate and with 1% SF. An addition of PF in the amount of 0.25% caused a reduction in the strength of the concrete by 7%.

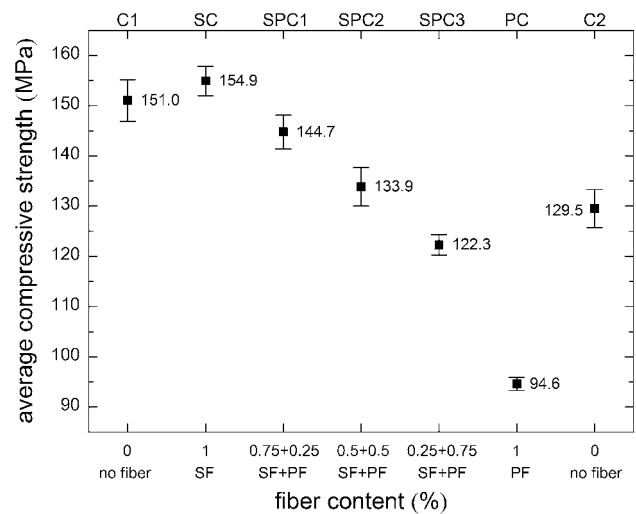


Fig. 2 Cube compressive strength

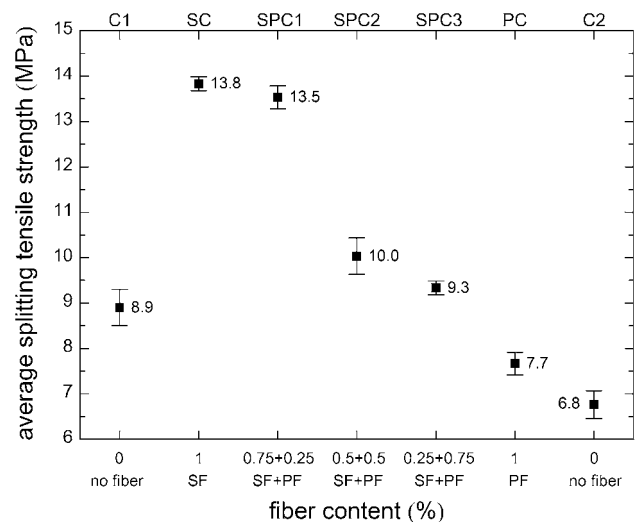


Fig. 3 Cube splitting tensile strength

3.2 Splitting Tensile Strength

The average values and error bars of cube splitting tensile strength are shown in Fig. 3.

The highest splitting tensile strength was achieved by the SC concrete with granodiorite aggregate and 1% SF. The SC cube strength grew by 37% in contrast to the C1 fiber-free cube. The addition of PF in the amount of 1% caused a rise in strength of the PC concrete by 14% compared to the UHPC without fibers. In other cases, the addition of PF lessens the splitting tensile strength. The results of the research illustrate that the use of fibers in any form or volume fraction resulted in a rise in the splitting tensile strength as compared to that of concrete without fibers.

3.3 Static and Dynamic Moduli of Elasticity

The average values and error bars of cylinder static and dynamic moduli of elasticity for each type of UHPC are shown in Fig. 4.

The modulus of elasticity was marginally affected by adding SF. This value grew with increasing percentages of volume, mostly owing to the high modulus of elasticity of SF. It is worth noting that in SC, the static modulus was 4% higher than that of C1. The modulus gradually declined with a lower content of steel fibers. The addition of PF in the amount of 1% resulted in a fall in the static modulus of elasticity by 10% in comparison to the C2 concrete without fibers. In the case of the concrete made with granite aggregate, the static modulus of elasticity of C2 compared with C1 made with granodiorite aggregate was lower by 15.2%.

Based on the findings (see Fig. 4), an adverse effect of the addition of PF on the dynamic modulus of elasticity can be observed. With an increasing amount of fibers from 0.25 to 1%, the dynamic modulus gradually drops. The dynamic modulus of elasticity of PC with 1% PF was the smallest and was 30% lower than that of SC with 1% ST.

3.4 Flexural Tensile Strength

The flexural strength depends on the quantity of SF and/or PF in UHPC. The average values and error bars of the flexural tensile strength are presented in Fig. 5.

The flexural tensile strength was notably influenced by adding steel and polypropylene fibers; nonetheless, the lowest strength was observed both when the percentage of PF volume added was the highest as well as for the concrete with granite aggregate without fibers. The lowest strength value is 1.73 times less than the maximum strength achieved by the concrete with 1% SF.

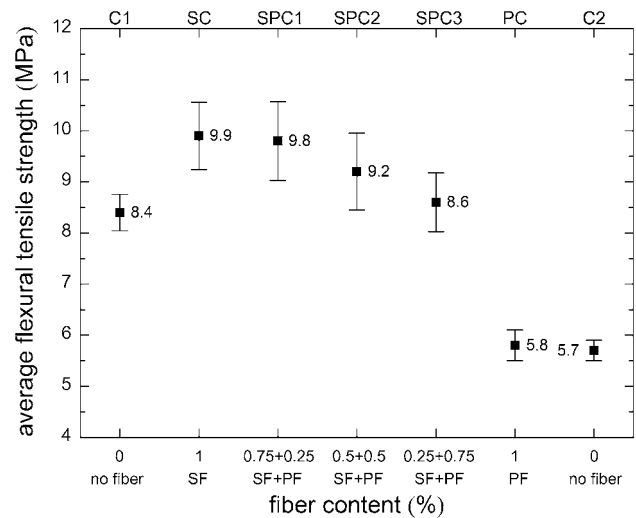


Fig. 5 Average flexural tensile strength

Typical experimental load–deflection curves for the notched specimens are shown in Fig. 6. During the first stage of examination, CMOD and deflection were measured until cracking of the beams along the whole height. After dismantling the strain gauge, only deflection was recorded.

The test curves were nearly linear up to the peak loads. The curves descended until the breaking point of the specimens. The fiber-reinforced UHPC specimens displayed a tri-linear plot. After reaching the peak load, the load carrying capacity declines; moreover, the lower the steel fiber content, the higher the loss of strength. As the micro-cracks grow and consolidate into larger macro-cracks, the long hooked-end fibers aid in bridging the cracks. In particular, the peak load for SPC2 is the highest and rose by 38%, compared to that of C2 (see Table 6). The amount of longitudinally oriented fibers ascertained obtaining peak load

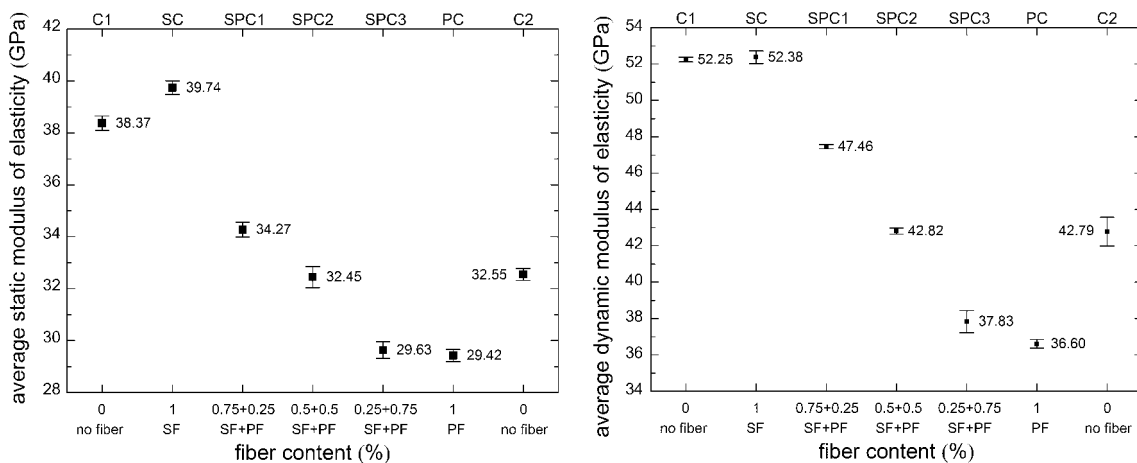


Fig. 4 Cylinder static and dynamic moduli of elasticity

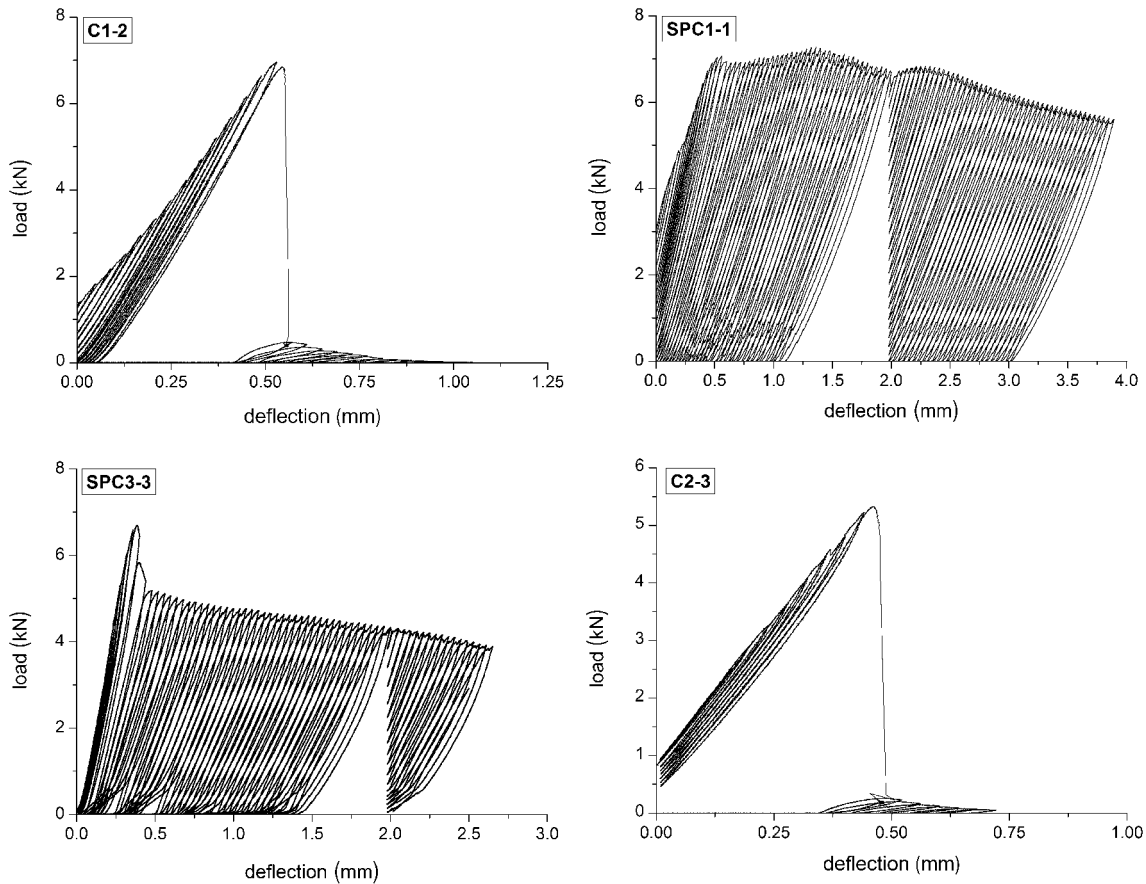


Fig. 6 Load–deflection curves for UHPC and hybrid fiber-reinforced UHPC notched specimens

values, as indicated by the very high coefficient of variation observed for the steel fiber-reinforced batch.

3.5 Fracture Energy

Only the impact of the fibers was taken under consideration when evaluating the equivalent flexural strength (hatched field— A_2 and grey field— A_3 in Fig. 7), whereas the amount of the energy required to fracture concrete corresponding to the OBA field (A_1) was omitted.

The results of the flexural tensile strength parameters are included in Table 6.

Citing the data given in Table 6, it can be seen that flexural strength values $f_{R,4}$ are higher than $f_{eq,3}$ only in the cases of using hybrid fiber UHPC with the exception of SPC3 concrete with the high volume of PF. For all the kinds of fibers, the equivalent flexural strength values are lower than the those at the limit of proportionality $f_{ict,L}$.

The fracture energy (G_F) was calculated as the area under the stress–displacement curves. The fracture energy for fiber reinforced UHPC needs to be computed in relation to a specified value of displacement. A reliable cut-off point can be selected at a displacement of 10 mm [34];

however, only a fracture dissipating up to a deflection of 3 mm is noteworthy from the designing perspective [35, 36], and such a deflection value was adopted while calculating the energy in this study. The average values and error bars of fracture energy for UHPC concretes are displayed in Fig. 8.

In the above-mentioned figure, the results are presented on a logarithmic scale. The greatest differences between the fracture energy values were noted for the UHPC and fiber-reinforced UHPC. The obtained results emphasize the impact of the fiber elasticity modulus on the variation of UHPC fracture properties. The studies have indicated that the most fracture resistant concrete was SC which had 1% SF, and this concrete has a fracture energy 531 times greater than that without SF. In the case of concrete with 1% PF, this energy is 565 times higher than the G_F of C2. C1 concrete based on granodiorite aggregate was characterized by energy 80% higher than that of the C2 concrete fabricated with granite aggregate. The fracture energy of hybrid concrete falls with a larger addition of PF. In the C1 and C2 samples, a brittle fracture occurred through separation of the beams into two parts. The fiber-reinforced UHPC samples with cracks underwent significant

Table 6 Average values of flexural tensile strength parameters

Type of UHPC	F_{max} (kN)	F_L (kN)	A_2 [kN × mm]	A_3 [kN × mm]	$f_{fc,t,L}$ (MPa)	$f_{eq,2}$ (MPa)	$f_{eq,3}$ (MPa)	$f_{R,1}$ (MPa)	$f_{R,4}$ (MPa)	K_{Ic} (MN/m ^{1.5})
C1	7.5	1.2	-	-	1.6	-	-	7.9	-	1.61
SC	8.8	5.0	3.08	19.80	6.6	8.1	10.4	8.3	7.2	-
SPC1	8.7	4.0	3.04	18.86	5.3	8.0	9.9	8.8	10.1	-
SPC2	8.2	2.1	3.04	24.09	2.8	8.0	12.7	8.4	13.0	-
SPC3	7.6	3.4	3.19	15.21	4.5	8.4	8.0	8.7	7.4	-
PC	5.2	4.2	1.18	4.57	5.5	3.1	2.4	3.0	1.6	-
C2	5.1	2.7	-	-	3.5	-	-	2.5	-	1.09

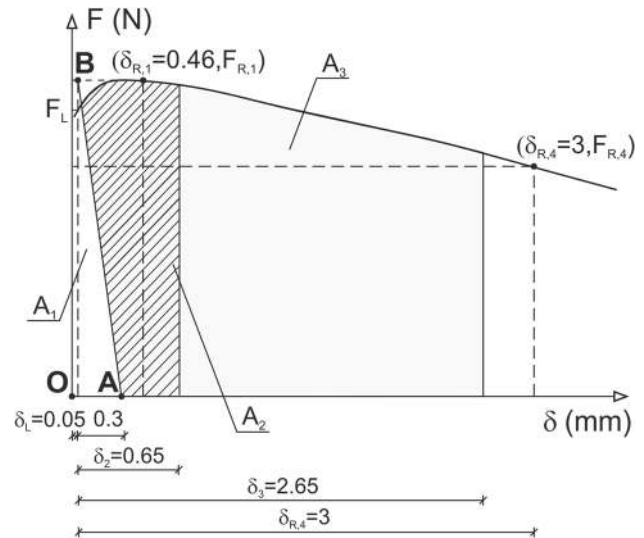


Fig. 7 Evaluation of flexural tensile strength for fiber-reinforced UHPC parameters

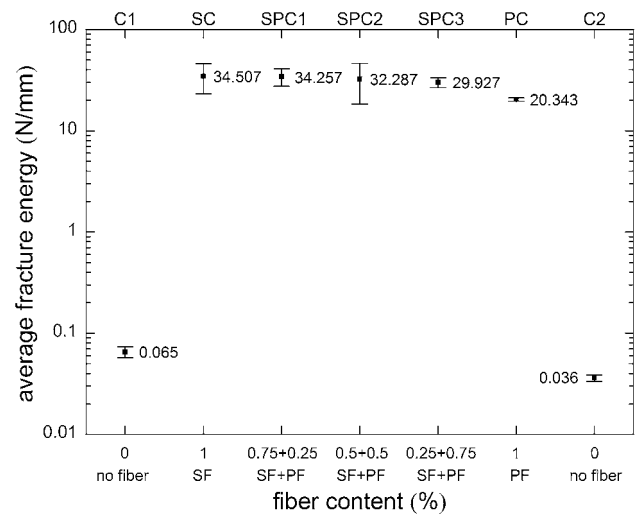


Fig. 8 Fracture energy (G_F) of UHPC with and without fibers

deflection; nonetheless, not in all cases did brittle destruction occur by samples breaking into two parts, since some bridges were formed by the fibers on the crack surface and limited the split. The samples with the fibers exhibited a more ductile behavior. The main crack went from the crack opening tip to the upper edge of the beam.

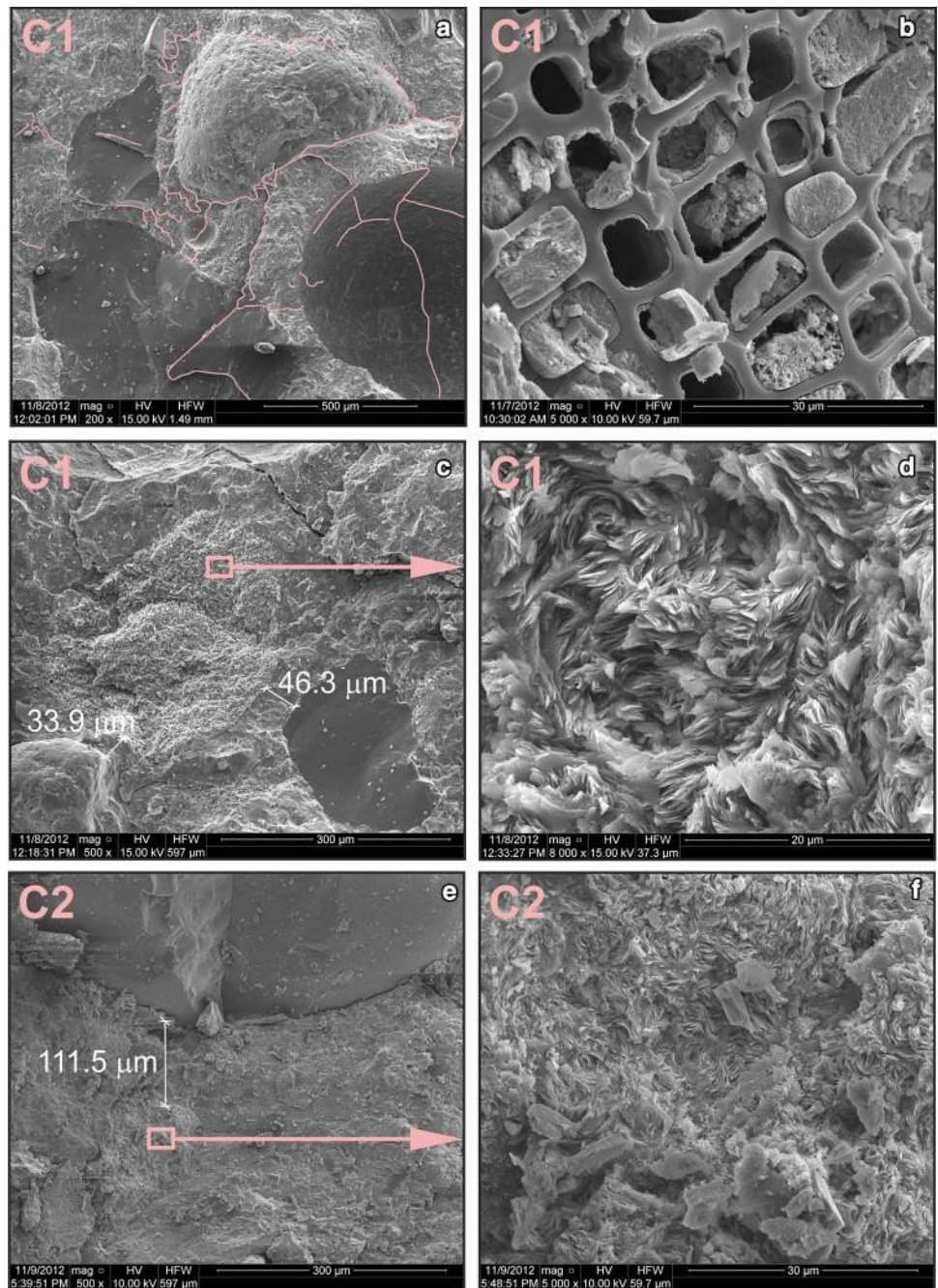
3.6 Microstructure

The toughness, splitting tensile strength, flexural tensile strength, and fracture energy of hybrid fiber-reinforced UHPC depend on the fiber surface, surface roughness, and bond strength between the aggregate and mortar.

To increase the bond strength, the W/C ratio needs to be reduced and an addition of silica fume is also required [37] as silica fume removes the discontinuity of pores and high content of portlandite crystals (CH) [38]. In UHPC, up to a value 60% of the ultimate stress, the cracks pass through the paste and the aggregate grains merge. Above this stress level, the cracks pass through the aggregate. A typical pattern of cracks is shown in Fig. 9a. In ordinary concrete, a layer of CH and C–S–H gel is formed directly on the aggregate grains. After the interfacial transitional zone (ITZ), reaching 40–50 μm, an area composed of

large CH and ettringite crystals with a higher porosity is formed. What is more, the CH crystals are oriented perpendicularly to the grain aggregate and overlap the C–S–H gel. It was observed in the UHPC concrete that a low W/B ratio creates a very dense microstructure in the hardened paste. Furthermore, the porosity is very low and the microstructure of the matrix surrounding the aggregate grains is composed mainly of homogeneous C–S–H gel. In addition, a C–S–H phase in the form of a honeycomb structure is found in UHPC (Fig. 9b). Nevertheless, CH or ettringite hardly occurs. The interfacial

Fig. 9 SEM image of UHPC microstructure



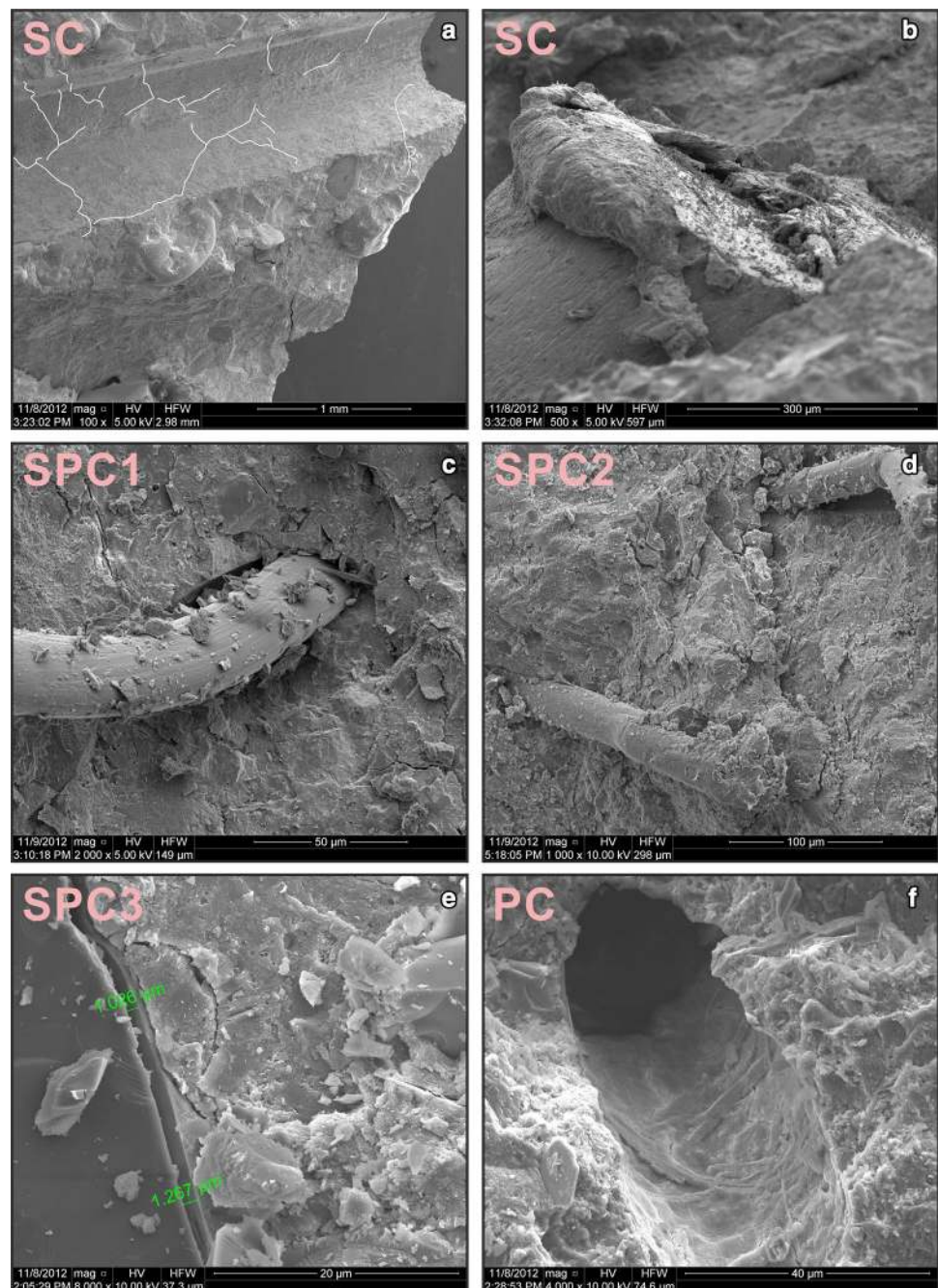
transitional zone reaches about 50 μm around the quartz sand grain, while around the coarse aggregate grain, it reaches about 100 μm (Fig. 9c, e). The C–S–H gel is converted to a tobermorite phase composed of plates formed into rosettes (Fig. 9c–f).

The steel fiber surface is rougher than the aggregate surface. Apart from reducing pores, this fiber boosts the bonding strength in the transitional contact zone between the SF and cement mortar. The high level of roughness and good adhesion between the SF and mortar is responsible for the dense mesh of micro-cracks formed at the contact surface

during fiber pull-out, as highlighted in Fig. 10a. The rough surface of the SF is shown in Fig. 10b.

Polypropylene fiber is a hydrocarbon polymer material. When PF is added to the cement paste, it results in the formation of a water film at the interface of the fiber and matrix. In view of the above-mentioned, one can conclude that the bond strength of the PF surface and matrix is poor, as shown in Fig. 10c, d. Moreover, the numerous pores between the PF and mortar lead to a notable increase in absorptivity, which was confirmed by tests in [39]. The absorption of water by UHPC with 1% SF was 100% less

Fig. 10 SEM image of fiber-reinforced UHPC microstructure



than that of concrete with 1% PF. Portlandite – calcium hydroxide macro-crystals can easily grow, making the transition zone more porous (Fig. 10f). It can be seen in Fig. 10d that the polypropylene fibers are mostly broken, and there were a few cases where PF were pulled out from the mortar (Fig. 10f), but without apparent damage to the contact surface.

4 Discussion

The results show a higher effectiveness of SF in boosting concrete strength. Based on the test results, dependencies and associations between the different concrete properties were proposed. The graph (Fig. 11) shows the dependence between compressive and splitting tensile strength for UHPC with fibers.

The compressive strength completely corresponds to the splitting tensile strength of UHPC with SF or/and PF. The polynomial trend was characterized by a good correlation coefficient $R^2=0.8801$ and relatively low errors in the intercept. The greatest difference was observed when comparing the UHPC with the maximum or higher volume of SF (SC, SPC1) and UHPC with only polypropylene fibers (PC). It is essential to point out that the type of aggregate had an influence on the data. The data for hybrid fiber-reinforced UHPC were obtained from the middle part of the curve. The relationship between the flexural tensile and splitting tensile strength for UHPC with fibers is presented in Fig. 12.

The relationship between the flexural tensile and splitting tensile strength for UHPC with fibers is presented in the form of the polynomial ax^2+bx+c . The high correlation coefficient equal to 0.909 indicates that the data have

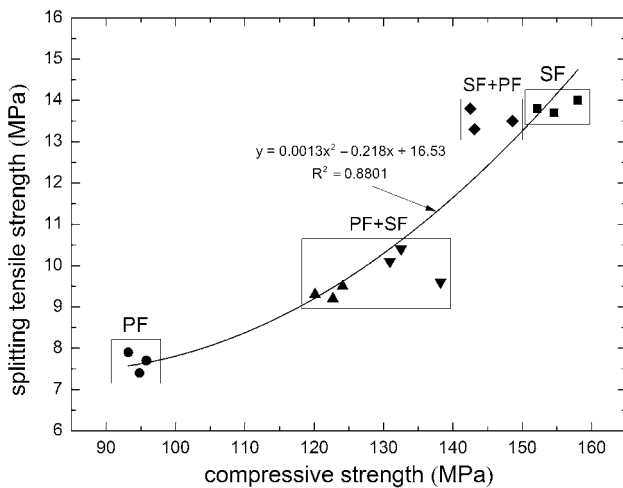


Fig. 11 Correlation between compressive strength and splitting tensile strength for fiber-reinforced UHPC

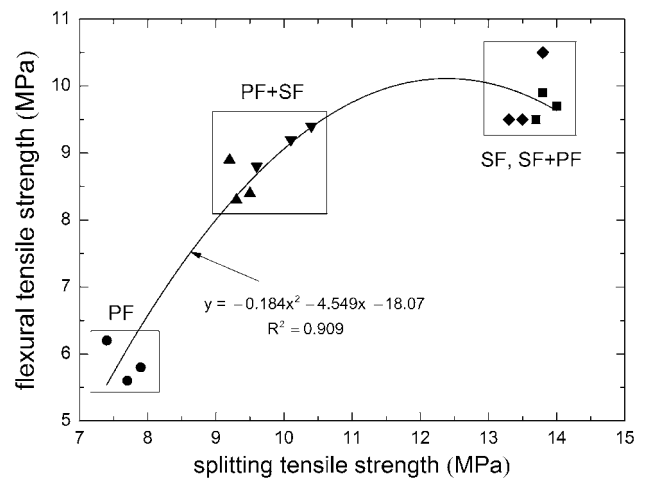


Fig. 12 Relationship between flexural and splitting tensile strength for fiber-reinforced UHPC

been matched by the best R^2 value (see Fig. 12). A higher correlation coefficient value indicates that flexural tensile strength has a strong association with splitting tensile strength. There is a clear grouping of the results depending on the type and quantity of fibers in the concrete, which was also remarked in the relationship between the compressive and splitting tensile strength (Fig. 11). The worst results were noticed for the UHPC with PF, and the best for SF and SF+PF. Figure 13 illustrates the dependence of the static and dynamic moduli of elasticity for all the tested concretes.

It was observed that the static modulus is completely congruous with the dynamic modulus. The polynomial trend was characterized by a good correlation coefficient $R^2=0.982$ and low errors in the intercept. The results

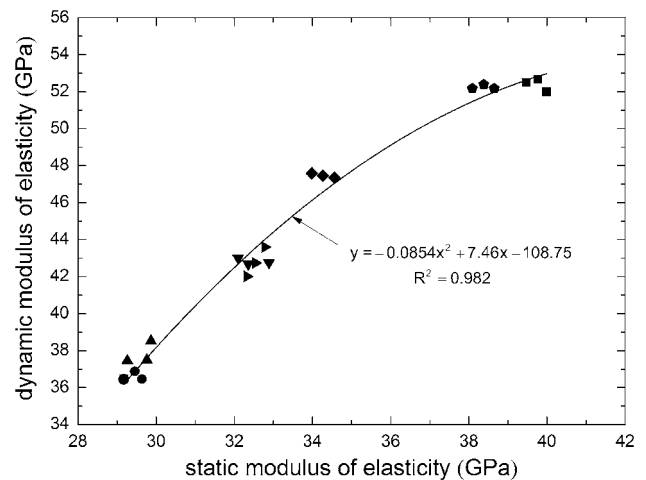


Fig. 13 Correlation between static and dynamic moduli of elasticity for UHPC

depend on the aggregate and fiber type, where the highest results were obtained for the UHPC with granodiorite aggregate without and with 1% SF, whereas the lowest results were achieved by the UHPC with granite aggregate containing PF in the amounts of 0.75 and 1%. Interestingly, the UHPC without fibers with granite aggregate obtained nearly the same parameters as the hybrid fiber-reinforced UHPC with SF in the amount of 0.5% and 0.5% PF. The relationship between the flexural strength and fracture energy for UHPC with fibers is presented in Fig. 14.

The linear relationship between the flexural tensile strength and fracture energy is presented in the form of $3.508x - 0.0585$. The high correlation coefficient equal to 0.999 indicates which means that the data have been matched by the best R^2 value (Fig. 14). A higher correlation coefficient value indicates that flexural strength has a strong relationship with fracture energy.

The effect of PF on compressive and flexural strength is not quite clear. A reduction in the compressive strength was achieved by substituting a portion of SF with PF as proved by the test results of hybrid fiber-reinforced concretes [16]. Large contents of PF are more difficult to disperse uniformly; therefore, the fibers tend to cluster and create more micro-defects in the cement matrix, reducing concrete compressive strength [40]. Particularly, the above-mentioned analyses can be associated with the results of the splitting tensile strength test. The strength rises by 10.5% when adding the smallest quantity of PF (0.5%), while a further addition results in a steep drop. In the case of other strength tests, the addition of fibers in each case also produces a decline in compressive strength, flexural strength, and modulus of elasticity. To take advantage of the maximum fiber strength and ameliorate the concrete properties, strengthening the PF interfacial bond is vital.

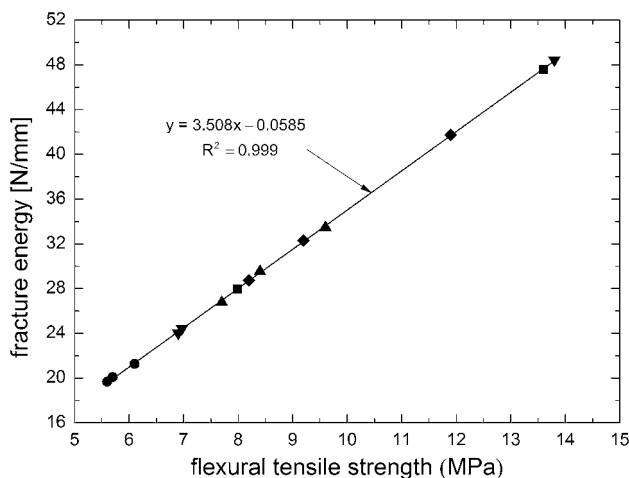


Fig. 14 Relationship between flexural tensile strength and fracture energy for fiber-reinforced UHPC

The advantageous qualities of steel fibers, such as the ability to restrain crack extension, reduce the extent of stress concentration at crack tips, change crack direction, and slow down the crack growth rate, all boost the compressive strength of concrete containing SF [41]. This is thanks to the higher strength and elastic modulus of steel fibers compared to those of PF.

The G_F values of UHPC with hybrid fibers are ascribed to the volume content of the low-modulus fibers. The higher the volume content of low-modulus fibers, the lower the G_F values obtained. The fact that the ductility of fiber-reinforced UHPC material at high levels of strain is highly dependent on the ability of the fibers to bridge the cracks is evidenced by the fracture energy results. The fact that the equations (see Table 5) involve both load and displacement explains the difference in the G_F values of the SF and PF difference in the G_F values of the SF and PF. The G_F values for high-modulus fibers will always be numerically higher than those for low-modulus fibers. It may well be that, in many cases, a combination of high-modulus SF and low-modulus PF may contribute more effectively to a longer period of durable service life. What is more, the stiffer SF provide higher resistance to loads, whereas PF of a low modulus of elasticity provide greater resistance to shrinkage and temperature stress.

The poor interfacial transition zone and weaker adhesion of PF to the matrix were brought on about by the high hydrophobicity of these fibers, which, in turn, increased the number of micro-cracks in the cement matrix (Fig. 15).

Although the width of micro-cracks of fiber-reinforced UHPC was appreciably influenced by SF and PF additions, the lowest width of micro-cracks occurred when the SF volume percentage was the highest. The widest micro-cracks range from 0.33 to 1.76 μm , and the C2 concrete

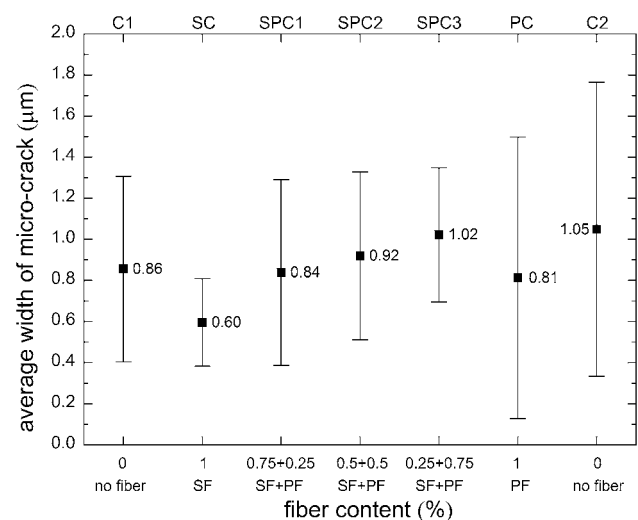


Fig. 15 Average width and error bars of micro-crack of all UHPC

without fibers with the granite aggregate had the highest average width of micro-cracks, whereas for C1, it is about 18% lower. An increased content of PF in hybrid reinforced UHPC creates expansion of the width of micro-cracks up to 41% (SPC3).

5 Conclusions

The mechanical properties, fracture energy, and micro-structure of UHPC and fiber-reinforced UHPC were investigated. Based on the results and discussions presented in this paper, the following conclusions can be drawn:

- The addition of SF and PF influenced all the tested mechanical properties of UHPC.
- SC concrete with 1% SF demonstrated the highest compressive strength. The steel fibers increased the compressive strength by about 2.6% at a 1% fiber volume content, while PF reduced the compression strength by about 57.3% at a 1% fiber volume content. The addition of SF in the amount of 0.5%, and PF amounting to 0.5% caused an increase in the compressive strength by only 3.3% as compared to C2.
- The splitting tensile strength of fiber-reinforced UHPC increased, depending on the steel fiber volume content, and was higher by 52, 47, and 37%, respectively, at 0.75, 0.5, and 0.25% SF volume. The concrete with 1% SF displayed the highest splitting tensile strength and was, in fact, higher by 55% than for the concrete without fibers.
- It was observed that the dynamic modulus completely correlated with the static modulus. The dynamic and static moduli of elasticity of PC with 1% PF were the smallest and were 20–30% lower than that of SC with 1% steel fibers. With an increasing addition of fibers from 0.25 to 1%, the dynamic modulus gradually decreases. The above-mentioned property was also affected by the type of coarse aggregate.
- The content of steel fibers had a notable impact on the flexural strength of fiber-reinforced UHPC. The experimental investigations indicated that the SF content had the greatest effect on the cracking resistance behavior of UHPC.
- The obtained results emphasized the effect of the fiber modulus of elasticity on the variation of UHPC fracture properties. The highest differences in fracture energy were observed between the UHPC and fiber-reinforced UHPC, whose fracture energy fell with increasing additions of PF. The most fracture resistant concrete was SC which had 1% SF.
- The microstructure investigations showed that SF reduced the pores and boosted the bonding strength in

the transitional contact zone between the SF and mortar. On the other hand, the bond strength on the PF surface was poor as evidenced by numerous pores between the PF and mortar. Enlargement of the average width of micro-cracks was brought about by increased contents of PF in the hybrid reinforced UHPC.

Acknowledgements This work was financially supported by the Ministry of Science and Higher Education—Poland, within the statutory research number S/15/B/1/2017, S/14/2017.

Open Access This article is distributed under the terms of the Creative Commons Attribution 4.0 International License (<http://creativecommons.org/licenses/by/4.0/>), which permits unrestricted use, distribution, and reproduction in any medium, provided you give appropriate credit to the original author(s) and the source, provide a link to the Creative Commons license, and indicate if changes were made.

References

1. Wang D, Shi C, Wu Z, Xiao J, Huang Z, Fang Z (2015) A review on ultra high performance concrete: Part II. Hydration, microstructure and properties. *Constr Build Mater* 96:368–377
2. fib, Structural Concrete. Textbook on behaviour, design and performance, 2nd edn, vol. 1, fib Bulletin 51, fédération internationale du béton, Lausanne 2009
3. IH Yang, C Joh, BS Kim (2010) Structural behavior of ultra high performance concrete beams subjected to bending. *Eng Struct* 32:3478–3487
4. Tuan NV, Ye G, van Breugel K, Copuroglu O (2011) Hydration and microstructure of ultra high performance concrete incorporating rice husk ash. *Cem Concr Res* 41:1104–1111
5. Tam CM, Tam Vivian WY, Ng KM (2012) Assessing drying shrinkage and water permeability of reactive powder concrete produced in Hong Kong. *Constr Build Mater* 26:79–89
6. Bonneau O, Vernet C, Moranvill M, Aïtcin PC (2000) Characterization of the granular packing and percolation threshold of reactive powder concrete. *Cem Concr Res* 30:1861–1867
7. Li X, Sun L, Zhou Y, Zhao S (2010) a review of steel-polypropylene hybrid fiber reinforced concrete. *Appl Mech Mater* 238:26–32
8. Xu Z (2003) Technology and application of fiber reinforced concrete. China Building Industry Press, Beijing
9. Prisco M (ed) (2007) Fibre-reinforced concrete for strong, durable and cost-saving structures and infrastructures. Brescia, Starrylink
10. Abdi MR, Mirzaeifar H (2016) Effects of discrete short polypropylene fibers on behavior of artificially cemented kaolinite. *Int J Civ Eng* 14:253–262
11. Bantia N, Gupta R (2006) Influence of polypropylene fiber geometry on cracking in concrete. *Cem Concr Res* 36:1263–1267
12. Zheng Z, Feldman D (1995) Synthetic fiber-reinforced concrete. *Prog Polym Sci* 20:185–210
13. Zhu YG, Kou SC, Poon CS, Dai JG, Li QY (2013) Influence of silane-based water repellent on the durability properties of recycled aggregate concrete. *Cem Concr Compos* 35:32–38
14. Afroughsabet V, Ozbakkaloglu T (2015) Mechanical and durability properties of high-strength concrete containing steel and polypropylene fibers. *Constr Build Mater* 94:73–82

15. Song PS, Hwang S, Sheu BC (2005) Strength properties of nylon-and polypropylene-fiber-reinforced concretes. *Cem Concr Res* 35(8):1546–1550
16. Sivakumar A, Santhanam M (2007) A quantitative study on the plastic shrinkage cracking in high strength hybrid fiber reinforced concrete. *Cem Concr Compos* 29(7):575–581
17. Nili M, Afroughsabet V (2012) Property assessment of steel-fiber reinforced concrete made with silica fume. *Constr Build Mater* 28(1):664–669
18. Zhang Y, Lv W, Peng H (2016) Shear resistance evaluation of strain-hardening cementitious composites member. *Int J Civ Eng* 1–7
19. Nili M, Azarioon A, Danesh A, Deihimi A (2016) Experimental study and modeling of fiber volume effects on frost resistance of fiber reinforced concrete. *Int J Civ Eng* 1–10
20. Ganesan N, Indira PV, Sabeena MV (2013) Tension stiffening and cracking of hybrid fiber-reinforced concrete. *ACI Mater J* 110(6):715–722
21. Dawood ET, Ramli M (2010) Development of high strength flowable mortar with hybrid fiber. *Constr Build Mater* 24(6):1043–1050
22. Yao W, Li J, Wu K (2003) Mechanical properties of hybrid fiber-reinforced concrete at low fiber volume fraction. *Cem Concr Res* 33(1):27–30
23. Banthia N, Majdzadeh F, Wu J, Bindiganavile V (2014) Fiber synergy in hybrid fiber reinforced concrete (HyFRC) in flexure and direct shear. *Cem Concr Compos* 48:91–97
24. RILEM TC 50-FMC (1985) Determination of the fracture energy of mortar and concrete by means of three-point bend tests on notched beams. *Mat Struct* 18:285–290
25. RILEM TC 89-FMT (1990) Size-effect method for determining fracture energy and process zone size of concrete. *Mat Struct* 23:461–465
26. ASTM C215-85 (1985) Standard Test method for fundamental transverse, longitudinal and torsional frequencies of concrete specimens, Annual Book of ASTM Standard, vol 04. 02, pp 117–120
27. Gettu R, Shah SP (1994) Fracture mechanics chapter in high performance concretes and applications. In: Shah SP, Ahmad SH (eds) Edward Arnold, London Melbourne Auckland
28. RILEM TC 162-TDF (2003) Test and design method for steel fibre reinforced concrete sigma-epsilon-design method. Final recommendation. *Mat Struct* 36:560–567
29. Giaccio G, Tobes JM, Zerbino R (2008) Use of small beams to obtain design parameters of fibre reinforced concrete. *Cem Concr Compos* 30:297–306
30. Barr BIG, Lee MK (2003) Round-robin analysis of the RILEM TC 162-TDF beam-bending test: Part 2—approximation from the CMOD response. *Mat Struct* 36:621–630
31. Barr BIG, Lee MK (2003) Round-robin analysis of the RILEM TC 162-TDF beam-bending test: Part 3—fibre distribution. *Mat Struct* 36:631–635
32. RILEM TC 162-TDF (2000) Test and design method for steel fibre reinforced concrete. Recommendations for bending test. *Mat Struct* 33(225):3–5
33. RILEM TC 162-TDF (2002) Test and design method for steel fibre reinforced concrete. Bending test. Final recommendation. *Mat Struct* 35(253):579–582
34. Ozalp F, Akkaya Y, Sengul C, Akcay B, Tasdemir MA, Kocaturk AN (2007) Curing effect on fracture of high-performance cement based composites with hybrid steel fibers. In: Proceedings of sixth international conference on fracture mechanics of concrete and concrete structures—FramCoS-6, Catania, Italy, 3, pp 1377–1385
35. Barros JAO, Pereira E, Ribeiro A, Cunha V (2005) Self-compacting steel fibre reinforced concrete for precast sandwich panels - experimental and numerical research, In: Proceedings of international workshop on advanced in fiber reinforced concrete, Bergamo, Italy, pp 169–180
36. Bencardino F, Rizutti L, Spadea G, Swamy RN (2010) Experimental evaluation of fiber reinforced concrete fracture properties. *Compos Part B* 41:17–24
37. Shi C, Wu Z, Xiao J, Wang D, Huang Z, Fang Z (2015) A review on ultra high performance concrete: Part I. Raw materials and mixture design. *Constr Build Mater* 101:741–751
38. Kurdowski W (2014) Cement and concrete chemistry. Springer, Netherlands
39. Barnat-Hunek D, Smarzewski P (2016) Influence of hydrophobisation on surface free energy of hybrid fiber reinforced ultra-high performance concrete. *Constr Build Mater* 102:367–377
40. Sadrmojtazi A, Fasihi A. Influence of polypropylene fibers on the performance of nano-sio2-incorporated mortar. *Iran J Sci Technol Trans B Eng* 34(B4):385–395
41. Yan H, Sun W, Chen H (1999) The effect of silica fume and steel fiber on the dynamic mechanical performance of high-strength concrete. *Cem Concr Res* 29(3):423–426